4528 *Biochemistry* **2009,** *48,* 4528–4537
DOI:10.1021/bi8021558

BIOCHEMISTRY
including biophysical chemistry & molecular biology
Article

Charge Stabilization and Entropy Reduction of Central Lysine Residues in Fructose-Bisphosphate Aldolase[†]

Miguel St-Jean,[§] Casimir Blonski,[‖] and Jurgen Sygusch*[,§]

[§]*Département de Biochimie, Université de Montréal, Montréal, Québec H3C 3J7, Canada, and* [‖]*Université de Toulouse, UPS, LSPCMIB (Laboratoire de Synthèse et Physico-Chimie de Molécules d'Intérêt Biologique), UMR CNRS 5068, 118, Route de Narbonne, F-31062 Toulouse Cedex 9, France*

Received November 21, 2008; Revised Manuscript Received April 8, 2009

ABSTRACT: Fructose-1,6-bisphosphate muscle aldolase is an essential glycolytic enzyme that catalyzes reversible carbon−carbon bond formation by cleaving fructose 1,6-bisphosphate to yield dihydroxyacetone phosphate (DHAP) and D-glyceraldehyde phosphate. To elucidate the mechanistic role of conserved amino acid Asp-33, Asn-33 and Ser-33 mutants were examined by kinetic and structural analyses. The mutations significantly compromised enzymatic activity and carbanion oxidation in presence of DHAP. Detailed structural analysis demonstrated that, like native crystals, Asp-33 mutant crystals, soaked in DHAP solutions, trapped Schiff base-derived intermediates covalently attached to Lys-229. The mutant structures, however, exhibited an abridged conformational change with the helical region (34−65) flanking the active site as well as pK_a reductions and increased side chain disorder by central lysine residues, Lys-107 and Lys-146. These changes directly affect their interaction with the C-terminal Tyr-363, consistent with the absence of active site binding by the C-terminal region in the presence of phosphate. Lys-146 pK_a reduction and side chain disorder would further compromise charge stabilization during C−C bond cleavage and proton transfer during enamine formation. These mechanistic impediments explain diminished catalytic activity and a reduced level of carbanion oxidation and are consistent with rate-determining proton transfer observed in the Asn-33 mutant. Asp-33 reduces the entropic cost and augments the enthalpic gain during catalysis by rigidifying Lys-107 and Lys-146, stabilizing their protonated forms, and promoting a conformational change triggered by substrate or obligate product binding, which lower kinetic barriers in C−C bond cleavage and Schiff base−enamine interconversion.

Aldolases are central enzymes that catalyze stereospecific carbon−carbon bond formation. Their role is best known in glycolysis where fructose-1,6-bis(phosphate) (FBP)[1] aldolases (EC 4.1.2.13) reversibly cleave FBP to yield triosephosphates, D-glyceraldehyde 3-phosphate (G3P), and dihydroxyacetone phosphate (DHAP). A common feature of class I aldolases is covalent catalysis involving formation of iminium (protonated Schiff base) between a lysine residue on the enzyme and a ketose substrate (*1*) that entails stereospecific proton exchange in the covalent intermediate (*2*). Of the three aldolase isozymes found in vertebrates (*3*), the catalytic mechanism has been most extensively studied using class I aldolase from rabbit muscle (*4*).

In the condensation direction, covalent intermediate formation takes place with the keto triosephosphate (DHAP) followed by condensation with the aldehyde (G3P) yielding the ketose of the acyclic FBP substrate (*5*, *6*) (Scheme 1). To form the C3−C4 bond of FBP, the enzyme stereospecifically abstracts the pro-*S* C3 proton of the trigonal iminium **1** (*7*, *8*) that is formed from the Michaelis complex with DHAP, thereby generating via the enamine **2** (*2*) the carbanionic character at C3 of DHAP (intermediate **3**) for the aldol reaction. The nascent carbon−carbon bond has the same orientation as the pro-*S* α-hydrogen initially abstracted from the DHAP imine intermediate (*9*). The new iminium intermediate formed is then hydrolyzed, and FBP is released according to the inverse reaction sequence shown in Scheme 1.

In class I aldolases, the active site is located at the bottom of a cleft in the center of its β-barrel fold and is accessible only from

[†]This research was supported by funding to J.S. from the Natural Science and Engineering Research Council (Canada) and Canadian Institutes for Health Research. C.B. was supported by funding from the European Commission (INCO) and CNRS (France). Work was carried out in part at beamlines X8C and X12B of the National Synchrotron Light Source, Brookhaven National Laboratory, which is supported by the U.S. Department of Energy, Division of Materials Sciences and Division of Chemical Sciences, under Contract DE-AC02-98CH10886. M.S. was the recipient of a Natural Science and Engineering Research Council (Canada) scholarship.

*To whom correspondence should be addressed. Phone: (514) 343-2389. Fax: (514) 343-2210. E-mail: jurgen.sygusch@umontreal.ca.

[1]Abbreviations: FBP, fructose 1,6-bis(phosphate); G3P, D-glyceraldehyde 3-phosphate; DHAP, dihydroxyacetone phosphate; D33N, Asp-33 → Asn mutant; D33S, Asp-33 → Ser mutant; WT, recombinant native; K107M, Lys-107 → Met mutant; K146A, Lys-146 → Ala mutant; K146M, Lys-146 → Met mutant; E187A, Glu-187 → Ala mutant; E187Q, Glu-187 → Gln mutant; WT-CP, carboxypeptidase A-treated aldolase; KIE, kinetic isotope effect; P_i, inorganic phosphate.

 Published on Web 4/8/2009

Scheme 1: Intermediates of the Catalytic Mechanism in Class I Aldolases

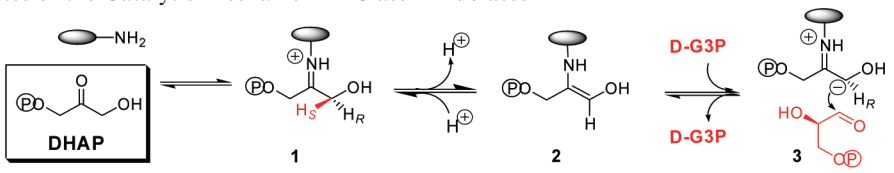

the carboxyl end of the β-strands comprising the β-barrel. The active site residues are highly conserved among eukaryotic class I aldolases sequenced to date (*10*), and there are a number of charged residues, vicinal to the Schiff base forming lysine, that participate in catalysis (*11*). Assignment of the role of charged active site residues is complex as these residues can mediate proton transfers by general acid/base catalysis, stabilize or destabilize charges, and because of their proximity to each other are susceptible to electrostatic modification of their pK_a values.

The crystal structures of reaction intermediates formed upon soaking native recombinant aldolase crystals with substrate, FBP, a substrate analogue, and with obligate product, DHAP, have significantly clarified our understanding of the mechanistic roles of active site residues (*12*, *13*). In the cleavage direction, substrate trapped as protonated Schiff base (iminium) showed reaction geometry consistent with incipient proton transfer to Glu-187 from the FBP C4 hydroxyl proton and which afforded stabilization of the developing negative charge on the C4 hydroxyl by Lys-146 that is within hydrogen bonding distance of the C4 hydroxyl (*12*). Glu-187 facilitated proton transfer in the ketimine intermediate, as indicated from crystal structures showing its interaction with the C2 hydroxyl of the carbinolamine analogue, (2*R*)-mannitol 1,6-bis(phosphate), while Asp-33 interacted with the C3 hydroxyl in both substrate and analogue (*12*). In the enamine intermediate, Asp-33 and Lys-146 form an ion pair and each residue hydrogen bonded with the C3 hydroxyl of DHAP (*13*). This sandwichlike interaction supported a planar geometry at DHAP atoms C1, C2, C3, and O3 and promoted resonance stabilization of the enamine intermediate. Binding of substrate and DHAP in rabbit muscle aldolase induced a conformational change in two helical regions flanking the active site that asymmetrically narrows the active site cleft, enabling Arg-303 to grasp the P1 phosphate moiety while Asp-33 interacts with the C3 hydroxyl of both substrate and DHAP (*12*, *13*). In the case of the substrate, the conformational displacement promotes the interaction of Ser-35 and Ser-38 with the P6 phosphate which is also stabilized by interaction with Lys-107.

A distinguishing structural feature of the enzyme is the C-terminal region (residues 343−363), specific to subunits of mammalian aldolases and their orthologues, that is relatively flexible, possessing an extended secondary structure, and adopts various conformations (*13*−*16*). The C-terminal region has a significant role in catalysis as loss of the conserved C-terminal Tyr-363 specifically inhibits stereospecific proton exchange in the Schiff base−enamine interconversion (*17*, *18*). The crystal structure of the Lys-146 → Met (K146M) mutant revealed active site docking by the C-terminal region in the presence of DHAP bound as a protonated Schiff base intermediate (*13*), and reaction geometry consistent with incipient stereospecific proton transfer between the C3-pro-*S* proton of DHAP in the iminium intermediate and Tyr-363. C-Terminal attachment to the active site is transient to minimize collision with the incoming G3P molecule during condensation as tight interaction by the C-terminal region

Scheme 2: Mechanism for Stereospecific Proton Transfer in the Protonated Imine at the Level of the DHAP Intermediate in the Active Site of Rabbit Muscle Aldolase

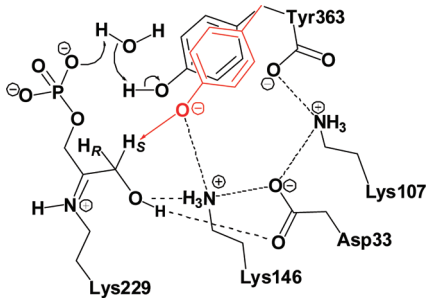

with the active site would block G3P binding and thus inhibit substrate formation (*13*). Phosphate binding at the P1 phosphate site traps the C-terminal region in the active site locus in a conformation identical as was observed in the K146M mutant, with the exception of the C-terminal Tyr-363 which makes an electrostatic interaction with Lys-146 that is precluded in the covalent DHAP intermediates (*13*). The concomitant conformational displacement by helix 34−52 guides C-terminal attachment in the active site by hydrogen bonding between Tyr-363 carboxylate and Ser-35.

The proton transfer mechanism, shown in Scheme 2, implicates prior activation of the Tyr-363 hydroxyl to yield a phenolate ion, which then abstracts the DHAP C3-pro-*S* proton. A key mechanistic feature facilitating the proton transfer is the role of Lys-146 in stabilizing the negative charge on the phenolate ion in the native structure (*13*). Indeed, the K146M mutation significantly inhibits enamine formation from the iminium (*13*) as well as cleavage activity (*19*), corroborating the interpretation of the structural data. Similarly, the D33A mutation significantly affects oxidation of the enamine intermediate by potassium hexacyanoferrate(III) and drastically compromises cleavage activity (*20*), alluding to an important function by Asp-33 in aldolase catalysis for which no mechanistic role has been established. Asp-33 is strategically positioned in the active site interacting with both Lys-146 and Lys-107, as shown in Scheme 2, and maintains these interactions in the protonated Schiff base and enamine complexes formed with FBP and DHAP, respectively.

To investigate the mechanistic role of Asp-33, two point mutations were selected that suppressed the negative charge on Asp-33 (D33N and D33S mutants), and the functional and structural differences of these Asp-33 mutants with respect to the native enzyme was probed at the molecular level using a combination of enzyme kinetics and crystal structure determination. Structure−function analysis indicated that Asp-33 mediates efficient substrate cleavage and proton transfer involving active site binding of the C-terminal region through a combination of charge stabilization and entropy reduction of the side chains of the central lysine residues, Lys-107 and Lys-146.

MATERIALS AND METHODS

Purification and Crystallization. Expression and purification of recombinant native (WT) and D33N, D33S, K107M, K146A, K146M, E187A, and E187Q mutant rabbit muscle aldolases were performed as described previously (*12*, *19*, *21*−*23*) using *Escherichia coli* strain BL21 SI for overexpression of the recombinant proteins (Invitrogen). The aldolase concentration was determined using an extinction coefficient of 0.91 cm mg^{-1} mL at 280 nm (*24*). D33N and D33S mutant aldolases were crystallized using the conditions reported previously (*12*). Carboxypeptidase A-treated aldolase (WT-CP) was prepared according to conditions described previously (*17*). Digestion of aldolase by carboxypeptidase A was monitored by the loss of enzymatic activity using a coupled assay and following NADH oxidation at 340 nm (*25*). The proteolyzed enzyme was separated from carboxypeptidase A by size exclusion chromatography when aldolase activity decreased to 5% of the original activity and corresponds to loss of the C-terminal Tyr-363 (*26*).

Kinetic Parameters and DHAP Oxidation. Aldolase catalysis was assessed by measuring substrate turnover over a FBP concentration range of 10 μM to 1 mM. Enzymatic activity for native and mutant enzymes was analyzed using Michaelis−Menten kinetics and kinetic parameters determined using GraFit (*27*). Estimated errors in kinetic parameters were less than 15% of the estimated value. DHAP carbanion/enamine intermediate formation was followed by oxidation of the intermediate with hexacyanoferrate(III) at saturating DHAP concentrations (10 mM), as reported previously (*28*−*31*). Measurements were taken in duplicate, and standard errors were estimated at 10% of measured oxidation rates.

Deuterated DHAP labeled at the C3-pro-*S* position was obtained by incubation of DHAP in D_2O in the presence of recombinant rabbit muscle aldolase (*29*). H−D exchange at the DHAP C3 position was monitored by ^{1}H NMR spectroscopy. The enzyme was discarded by ultrafiltration using Centricon P-10 ultrafiltration cartridges, and the concentration of deuteriated DHAP was determined enzymatically.

Crystallographic Data Collection and Processing. D33N and D33S mutant aldolase crystals were soaked for 10 min in ligand buffer containing DHAP (mother liquor with 20 mM DHAP) or in inorganic phosphate (P_i) buffer (mother liquor with 20 mM NaH_2PO_4). Prior to data collection, single crystals were cryoprotected in the ligand buffer containing 15% glycerol and immediately flash-cooled in a stream of gaseous N_2 cooled to 100 K. Data collections were performed on beamlines X8C and X12B of the National Synchrotron Light Source (Brookhaven National Laboratory, Upton, NY), and diffracted intensities were measured using a Quantum4 charge-coupled device detector (Area Detector Systems, Poway, CA). All data sets were processed with HKL2000 (*32*), and the results are summarized in Table 1.

Structure Determination and Refinement. All mutant crystal structures were isomorphous with the crystal structure of native aldolase and belonged to monoclinic space group $P2_1$. Structures were determined by difference electron density maps using the native aldolase homotetramer structure as a reference model [Protein Data Bank (PDB) entry 1ZAH] (*12*). Each asymmetric unit contains one homotetramer, consistent with the biologically active form of the enzyme. Refinement was performed as reported previously (*12*) with Crystallography and NMR System [CNS (*33*)] and O (*34*) and using all reflections having an $I/\sigma(I)$ of >1; however, electron density maps were calculated to the resolution indicated in Table 1 to ensure at least ~80% completeness in the highest-resolution shell with an $I/\sigma(I)$ of >2. The PRODRG server was used to generate ligand topology and parameter files (*35*). The presence of ligands in the final models was confirmed by inspection of simulated annealing $F_o - F_c$ omit maps. Final model statistics, calculated with CNS and PROCHECK (*36*), are listed in Table 1. The atomic coordinates and structure factors for D33N and D33S mutants of native, DHAP-bound, and phosphate-bound rabbit muscle aldolase have been deposited with the Protein Data Bank (PDB entries 3DFN, 3DFO, 3DFP, 3DFQ, 3DFS, and 3DFT, respectively). The final structure models have R_{cryst} (R_{free}) values of 0.141 (0.188), 0.152 (0.199), 0.156 (0.214), 0.150 (0.188), 0.141 (0.187), and 0.149 (0.205), respectively. The corresponding positional errors in atomic coordinates using Luzzati plots were estimated to be 0.15, 0.18, 0.19, 0.16, 0.16, and 0.17 Å, respectively. Errors in hydrogen bond distances and positional differences are reported as standard deviations and were estimated on the basis of their value in each subunit of the aldolase homotetramers unless specified otherwise. All figures were prepared using PyMOL (*37*). Superpositions were also performed with PyMOL overlaying Cα atom coordinates of aldolase residues 158−259, which are invariant to binding events as noted previously (*12*).

Orientations of carboxamide moieties of Asn residues for both D33N and D33S mutant structures were validated using the GLN and ASN B-factor Outliers option in COOT (*38*). Inspection of difference electron density omit maps set to high electron density level (10σ) unambiguously distinguished the correct carboxamide orientation of Asn-33. The electron density about the carboxamide O atom clearly exceeded the electron density at its N atom in all subunits which is consistent with an oxygen atom possessing a greater electron density than a nitrogen atom. The validated carboxamide orientation of Asn-33 retained the hydrogen bonding interaction as observed with the carboxylate moiety of Asp-33, where the Asp-33 OD1 atom formed a hydrogen bond with its backbone amide corroborating the interaction propensity of Asn residues with their backbone amides (*39*). This spatial orientation also enabled a favorable contact between Asn-33 ND2 and its backbone carbonyl.

The chemical identity of covalent intermediates trapped in the D33N−DHAP and D33S−DHAP structures was based on occupancy refinement with CNS using enamine and iminium intermediates built as alternate conformations. In each case, occupancy refinement yielded a dominant DHAP intermediate corresponding to a refined occupancy of >0.7 that was selected for further refinement as the fully occupied intermediate. Visual inspection of simulated annealing $F_o - F_c$ electron density omit maps corroborated the presence and selection of the modeled DHAP intermediates in each active site. The enamine and iminium intermediates can be distinguished at high resolution on the basis of their electron density shape because of their obligatory state of hybridization; in the enamine, Lys-229 Nζ is sp^3 hybridized, coincidental with an electron density that is nonplanar in shape due to the tetrahedral stereochemistry about Lys-229 Nζ, while in the iminium, sp^2 hybridization at Lys-229 Nζ results in an electron density that is planar in shape.

Modeling of the aldolase C-terminal region into the active site of D33N−P_i and D33S−P_i structures used subunit D of the WT−P_i structure which was superposed onto the same subunit of each mutant structure. Subunit D in the native enzyme has the

Table 1: Data Collection and Refinement Statistics

	D33N	D33N−DHAP	D33N−P_i	D33S	D33S−DHAP	D33S−P_i
Data Collection						
resolution[a] (Å)	44−1.86 (1.94−1.86)	44−1.94 (2.03−1.94)	50−2.05 (2.14−2.05)	35−1.82 (1.90−1.82)	44−2.03 (2.13−2.03)	50−1.94 (2.03−1.94)
wavelength[a] (Å)	1.100	1.100	1.100	1.100	1.100	1.100
no. of unique reflections/redundancy[a]	113592 (10312)/3.1 (1.9)	102675 (11031)/3.5 (2.3)	90937 (10688)/4.8 (3.9)	124981 (13297)/3.0 (2.1)	90924 (11803)/3.6 (3.2)	104376 (11363)/3.3 (2.2)
completeness[a] (%)	94.4 (77.3)	97.7 (84.2)	97.1 (91.5)	97.4 (83.4)	97.1 (88.7)	97.8 (85.6)
average $I/\sigma(I)$[a]	11.9 (2.2)	13.4 (2.2)	9.1 (2.3)	18.0 (3.5)	19.1 (5.9)	13.1 (2.2)
R_{sym}[a,b]	0.069 (0.257)	0.083 (0.430)	0.145 (0.806)	0.055 (0.216)	0.065 (0.195)	0.079 (0.404)
space group	$P2_1$	$P2_1$	$P2_1$	$P2_1$	$P2_1$	$P2_1$
unit cell parameters						
a (Å), b (Å), c (Å), β (deg)	84.2, 103.9, 84.9, 98.9	83.7, 103.1, 84.6, 98.7	85.0, 104.6, 85.8, 98.9	83.9, 103.7, 84.8, 98.8	83.9, 103.8, 84.8, 98.9	83.9, 103.6, 84.9, 98.7
Refinement						
no. of atoms						
protein	10813	10780	10813	10805	10759	10754
water	2265	2079	2104	2278	2120	2219
hetero	0	36	20	0	36	20
σ cutoff $\langle I/\sigma(I)\rangle$	1	1	1	1	1	1
R_{cryst} (%)[c]	14.1	15.2	15.6	15.0	14.1	14.9
R_{free} (%)[d]	18.8	19.9	21.4	18.8	18.7	20.5
root-mean-square deviation						
bond lengths (Å)	0.005	0.005	0.005	0.004	0.005	0.005
bond angles (deg)	1.201	1.236	1.206	1.208	1.216	1.242
average B-factor (Å^2)	21.5	25.2	21.9	22.6	20.5	23.0
Ramachandran analysis[e] (%)						
most favorable	91.9	91.6	91.7	92.7	92.5	91.5
allowed	8.1	8.4	8.3	7.3	7.5	8.5
Luzzati positional error (Å)	0.15	0.18	0.19	0.16	0.16	0.17

[a] All values in parentheses are given for the highest-resolution shell. [b] $R_{sym} = \sum_{hkl}\sum_i |I_i(hkl) - \bar{I}_i(hkl)|/\sum_{hkl}\sum_i I_i(hkl)$, with i running over the number of independent observations of reflection hkl. [c] $R_{cryst} = \sum_{hkl}||I_o(hkl)| - |I_c(hkl)||/\sum_{hkl}|I_o(hkl)|$. [d] $R_{free} = \sum_{hkl\in T}||I_o(hkl)| - |I_c(hkl)||/\sum_{hkl\in T}|I_o(hkl)|$, where T is a test data set randomly selected from the observed reflections prior to refinement. The test data set was not used throughout refinement and contained 8, 9, 9, 9, 9, and 9% of the total unique reflections for D33N, D33N−DHAP, D33N−P_i, D33S, D33S−DHAP, and D33S−P_i, respectively. [e] Analyzed by PROCHECK (*31*).

C-terminal region fully bound in the active site in the presence of phosphate (*13*). Controls superposing all atoms in quaternary structures of unliganded D33N and D33S structures yielded an rmsd value of < 0.2 Å, and pairwise superposition of unliganded mutant structures with quaternary structures of phosphate-soaked D33N and D33S structures yielded rmsd values of < 0.35 Å. Only N-terminal residues 1−10 and C-terminal residues 344−363 were omitted from these superpositions. The rmsd values were nearly identical to the calculated combined atomic position error derived from Luzzati plots of respective structures and indicate comparison of identical quaternary structures.

RESULTS AND DISCUSSION

Catalytic Activity. Michaelis−Menten kinetics were used to analyze initial rate velocities measured for site-directed mutations of charged residues proximal to the covalent intermediates, and the corresponding kinetic parameters are listed in Table 2. The mutations of residues Glu-187 and Lys-146, which have multiple roles in the aldolase reaction, significantly inhibited catalytic activity (*12*, *13*, *19*, *22*). The mutations, D33N and D33S, drastically reduced the rate of turnover but did not impact substrate binding, consistent with mechanistic roles in catalysis. To acquire additional insight into the role of Asp-33, turnover of the DHAP carbanion/enamine intermediate was assessed by oxidation with hexacyanoferrate(III) (*21*, *27*, *29*, *30*). Oxidation rates were diminished for all active site mutations (Table 3); however, oxidation rates were significantly greater than those for substrate cleavage, and is not inconsistent with the point mutations affecting multiple steps in the aldolase reaction mechanism. The low oxidation rate, observed for native aldolase, is a consequence of rate-limiting dissociation of the oxidation reaction product, 3-hydroxypyruvaldehyde phosphate, in the native enzyme (*40*). Oxidation rates using DHAP labeled with deuterium at the C3-pro-*S* hydrogen position were then compared with unlabeled DHAP to assess whether proton transfer was rate-limiting in Schiff base to enamine conversion (Table 3). The oxidation rates show a significant primary deuterium KIE for both Asp-33 mutants (Table 3), and indicating that stereospecific proton transfer of the C3-pro-*S* hydrogen of DHAP has become nearly rate-limiting for the D33N mutant; the rate reduction is ~300-fold compared to that of the native enzyme (*41*). The increase in primary KIE for the carboxypeptidase-treated enzyme is consistent with the participation of the C-terminal Tyr-363 in proton transfer (*13*, *42*).

A direct role of Asp-33 in proton transfer would be difficult to reconcile on the basis of the active site geometry where the residue is positioned in the native enzyme vicinal to the *re* face of the enamine (*13*) (cf. Scheme 2). This geometry would imply a preference for stereospecific proton transfer of the DHAP C3-pro-*R* proton. Although rotation about the C2−C3 bond is feasible in the Schiff base intermediate and would place the C3-pro-*S* proton proximal to Asp-33, this would require breakage of two hydrogen bonds formed by Lys-146 and Asp-33 with the DHAP C3 hydroxyl, depicted in Scheme 2. To acquire further insight, crystal structures of the Asp-33 mutants were determined bound in the presence of DHAP.

Covalent Intermediates. Flash cooling of D33N and D33S aldolase crystals in the presence of DHAP trapped a covalent intermediate in each subunit. Continuous electron density extending beyond Lys-229 Nζ (Figure 1) indicates formation of stable covalent adducts with DHAP and is compatible with binding of either an iminium and/or enamine intermediate. In the D33N−DHAP complex structure, refinement was consistent with two subunits having DHAP bound as a Schiff base intermediate (Figure 1A) while the remaining two subunits bound DHAP in the enamine form (Figure 1B). In the D33S−DHAP complex structure, all subunits contained DHAP bound predominantly as a Schiff base intermediate (Figure 1C). Comparison of average *B*-factors between bound DHAP and interacting side chains indicates near full active site occupancy by DHAP in both mutants. Active site integrity was not perturbed by the Asp-33 mutations when compared with the native enzyme bound by DHAP (rmsd Cα ~ 0.37 and 0.33 Å in D33N and D33S mutants, respectively). Comparison also revealed no significant positional differences among residues considered invariant to binding events. DHAP induces conformational changes in helical regions

Table 2: Kinetic Parameters of the FBP Cleavage Reaction for Recombinant Native and Mutant Aldolases of Active Site Residues Asp-33, Lys-107, Lys-146, and Glu-187

enzyme	k_{cat} (s^{-1})	K_m (μM)
WT	13.22	5.1
WT-CP	0.66	2.0
D33N	0.003	4.2
D33S	0.002	8.4
E187A	0.046	6.1
E187Q	0.005	13.4
K107M	0.65	41.2
K146A (*22*)	< 0.0002	ND[a]
K146M	0.0019	20.4

[a] Not determined.

Table 3: Carbanion Oxidation Rates for Recombinant Native and Mutant Aldolases As Shown in Table 1 Measured with Hexacyanoferrate(III) in the Presence of 10 mM DHAP

enzyme	DHAP oxidation rate (s^{-1})	(*S*)-[3-$^2H_1$]DHAP oxidation rate (s^{-1})	KIE[a]
WT	2.2	2.1	1.05
WT-CP[b]	2.2	0.9	2.4
D33N	0.050	0.010	5.0
D33S	0.083	0.027	3.1
E187A	0.200	0.184	1.1
E187Q	0.100	0.093	1.1
K107M	0.570	0.390	1.5
K146A	0.025	0.022	1.1
K146M	0.106	0.070	1.5

[a] Kinetic isotope effect represented as the ratio of DHAP oxidation rate to (*S*)-[3-^{2}H]DHAP oxidation rate. [b] Recombinant native aldolase treated with carboxypeptidase A as described in Materials and Methods.

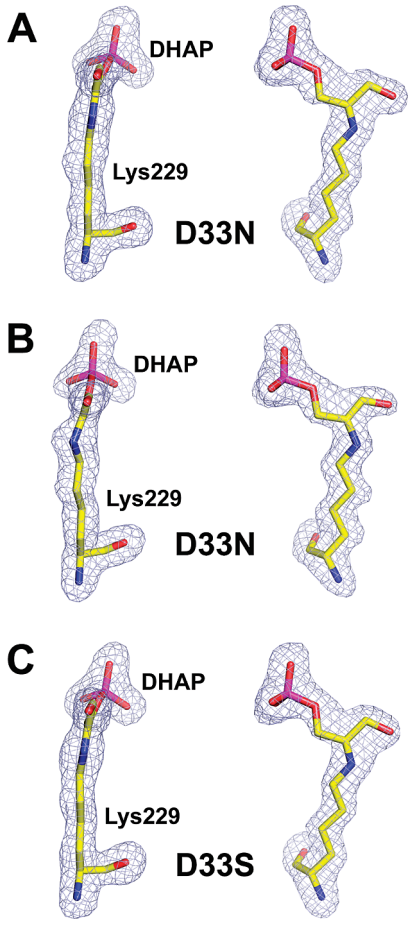

FIGURE 1: DHAP covalent intermediates trapped in the active site of D33N and D33S mutant rabbit muscle aldolases. In the D33N mutant, DHAP is covalently bound to Lys-229 as an iminium intermediate with electron density showing sp^2 hybridization or planar stereochemistry at Lys-229 Nζ, in two subunits (A), and as an enamine intermediate in the other two subunits consistent with an electron density that is nonplanar or tetrahedral geometry at Lys-229 Nζ (B). In the D33S mutant, DHAP is bound as an iminium intermediate in all subunits (C). Difference electron densities were calculated from 1.94 Å (D33N) and 2.03 Å (D33S) resolution simulated annealing $F_o - F_c$ omit maps encompassing Lys-229 and DHAP and contoured at 4.0σ.

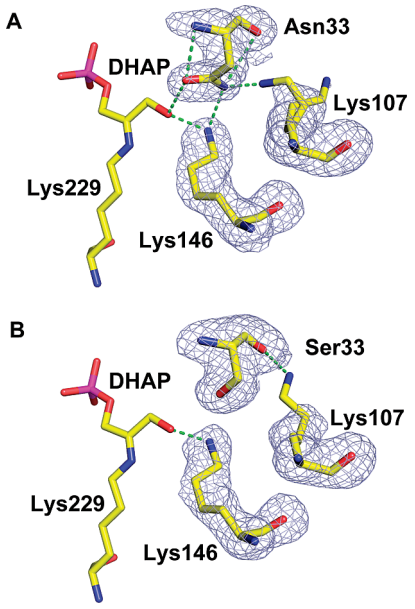

FIGURE 2: Active site organization of central lysine residues in the DHAP covalent intermediate for D33N and D33S mutants of native rabbit muscle aldolase. In the D33N mutant, Lys-146 interacts with DHAP and Asn-33 while Lys-107 exhibits alternate conformations, one of which interacts with Asn-33 (A). In the D33S mutant, Lys-146 interacts only with DHAP and the Lys-107 side chain exhibits higher *B*-factors interacting primarily with the Ser-33 backbone carbonyl (B). Difference electron densities were calculated from 1.94 Å (D33N) and 2.03 Å (D33S) resolution simulated annealing $F_o - F_c$ omit maps encompassing the Asp-33 mutation, Lys-107, and Lys-146 and contoured at 3.0σ.

of residues 34−65 and 302−315 in aldolase subunits of both mutants, which asymmetrically narrows the active site cleft, also observed in the structures of covalent intermediates formed by the native enzyme with FBP and DHAP (*12*, *13*). The magnitudes of the backbone conformational displacements in D33N and D33S mutants were, however, 50% smaller when compared to that of native aldolase (*12*, *13*) and indicate that the Asp-33 negative charge is requisite for full conformational displacement of these helical regions.

Interactions with active site residues that stabilize the covalent intermediates were identical to those found in the structures of the iminium and enamine intermediates formed in the K146 mutant and native enzyme, respectively (*13*), and include an unusually short hydrogen bond between the Ser-271 side chain and phosphate oxyanion (2.46 ± 0.07 and 2.31 ± 0.02 Å for D33N and D33S mutants, respectively). Asn-33 and Lys-146 further stabilize the covalent intermediates by hydrogen bonding the DHAP C3 hydroxyl (Figure 2A). The presence of a short hydrogen bond between Lys-146 and the DHAP C3 hydroxyl (2.38 ± 0.08 and 2.50 ± 0.2 Å for D33N and D33S mutants, respectively) (Figure 2A,B) is surprising given its absence in the native enamine structure (2.82 ± 0.05 Å). Although the parametrization of the force field model used in the structure refinement could result in a refinement artifact, the mutations, D33N and D33S, would increase active site hydrophobicity (*43*) which can strengthen hydrogen bonding by vicinal hydrogen bonding acceptors and donors (*44*) and would be consistent with formation of a short hydrogen bond.

Compared to those of other interacting lysine residues not found in the active site, the electron density of Lys-146 faded progressively in the direction of the Lys-146 Nζ atom along its side chain in both mutant structures. The electron density decrease for Lys-107 was even greater along its side chain when compared to that of Lys-146 (Figure 2A). In addition, Lys-107 exhibited more than one side chain conformer, and *B*-factors for Lys-107 exhibited even greater positional disorder compared to Lys-146, with the highest degree of disorder in the D33S mutant (Table 4). *B*-Factors of other active site residues proximal to the covalent intermediate were comparable (12 ± 3 $Å^2$) with respect to the native enamine intermediate (16 ± 3 $Å^2$). In both structures, the DHAP C3-pro-*R* position faces the mutated residue.

The Lys-107−Lys-146 distance showed considerable variation (from 3.7 to 7.3 Å) because of the different orientations of the Lys-107 side chain conformers, compared to a single precise distance of 4.24 ± 0.06 Å in the enamine intermediate of the native enzyme. At the shortest distance in the D33N mutant, both Lys-107 and Lys-146 are hydrogen bonded to the amide of the carboxamide moiety of Asn-33 (2.66 and 3.05 Å, respectively), and the consistency of the hydrogen bonding pattern requires that both lysine residues be unprotonated for each lysine Nζ

Table 4: *B*-Factors of Active Site Lysine Residues in Recombinant Native and Mutant Rabbit Muscle Aldolases

	B-factor (Å^2)					
structure	Lys-229 Cα atom	Lys-229 Nζ atom	Lys-146 Cα atom	Lys-146 Nζ atom	Lys-107 Cα atom	Lys-107 Nζ atom
WT (*12*)	13 ± 2	17 ± 2	17 ± 2	34 ± 4	17 ± 2	27 ± 4
WT−DHAP (*13*)	13 ± 3	20 ± 3	15 ± 2	21 ± 4	16 ± 2	18 ± 3
WT−P_i (*13*)	15 ± 2	18 ± 6	19 ± 1	29 ± 4	19 ± 1	27 ± 3
D33N	8 ± 2	15 ± 2	11 ± 1[a]	24 ± 3[a]	11 ± 3	48 ± 10
D33N−DHAP	13 ± 1	22 ± 3	15 ± 1	36 ± 8	15 ± 2[a]	36 ± 6[a]
D33N−P_i	9 ± 1	15 ± 1	11 ± 3[a]	21 ± 6[a]	12 ± 2	45 ± 16
D33S	10 ± 2	21 ± 3	12 ± 1[a]	29 ± 7[a]	13 ± 2	45 ± 8
D33S−DHAP	8 ± 1	23 ± 7	14 ± 2	51 ± 13	11 ± 1	58 ± 6
D33S−P_i	10 ± 1	19 ± 5	13 ± 2	21 ± 5	12 ± 2	47 ± 8
K146M−DHAP (*13*)	14 ± 1	21 ± 2	17 ± 2[b]	26 ± 4[c]	16 ± 1	22 ± 4[d]

[a] Multiple conformations in several subunits. [b] Met-146 Cα atom. [c] Met-146 Cε atom. [d] Multiple conformations in one subunit.

atom to accept a hydrogen bond from the Asn-33 amide ND2 atom (Figure 2A), in view of its significantly higher pK_a, making it unlikely to accept a hydrogen bond. The shorter interatomic distance between the lysine residues compared to the native enzyme supports diminished electrostatic repulsion due to their unprotonated state that would enable closer mutual approach. At the greatest separation, Lys-146 remains unprotonated, hydrogen bonding with Asn-33. Lys-146 is also close to Glu-187 (3.38 ± 0.09 Å) in the D33N mutant, while it makes no such close contact in the D33S mutant (4.29 ± 0.59 Å). The absence of steric hindrance to potential interaction by Lys-146 with Glu-187 supports the possibility that Lys-146 is not protonated in either Asp-33 mutant.

Electrostatic interactions such as those formed between Asp-33 and lysine residues 107 and 146 should increase the likelihood of these lysine residues to ionize (*43*, *45*). Affinity labeling studies on the native enzyme, however, indicate reduced pK_a values for Lys-146 of ~8.5 (*46*) as well as for Lys-107 of ~8.0 (*19*) which are consistent with electrostatic destabilization of the lysine pK_a values due to their spatial proximity (*47*−*49*). Although solvent accessibility by the lysine residues would mitigate significant reductions in their pK_a values, the hydrogen bonding interaction by both lysine residues with Asn-33 in this mutant implies a further pK_a reduction by Lys-107 and Lys-146 such that both residues become significantly unprotonated at pH 7.5 of the crystallization buffer, and enabling these residues to accept hydrogen bonds from Asn-33. In the D33S mutant where from the structural data Ser-33 is unable to hydrogen bond with either lysine residue (Figure 2B), charge destabilization would not necessitate simultaneous pK_a reductions in both Lys-107 and Lys-146. The intervening negative charge of Asp-33 in the native enzyme thus offsets substantial electrostatic destabilization due to the spatial proximity between Lys-146 and Lys-107 and results in only slightly basic pK_a values for the lysine residues at physiological pH.

The unprotonated form of Lys-146 in the covalent intermediate would furthermore not stabilize the negative charge transiently generated during C3−C4 bond cleavage at the C4 hydroxyl in the Schiff base complex formed with substrate (*12*). A predominantly uncharged Lys-146 would thus compromise cleavage of the C3−C4 bond and is consistent with a reduced rate of substrate turnover.

Phosphate Binding. D33N and D33S mutant aldolase crystals were soaked in phosphate buffer and flash-cooled in investigating whether a decrease in carbanion oxidation rates for

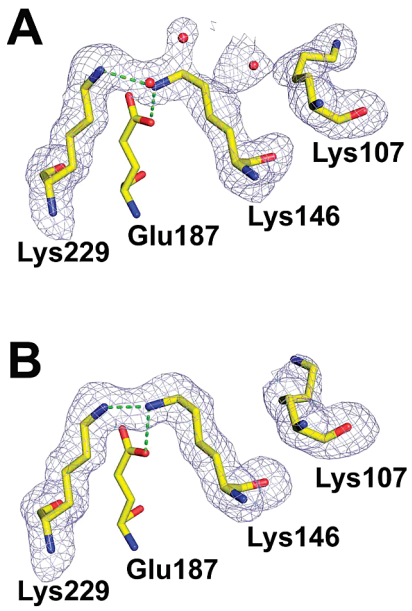

FIGURE 3: Aldolase active site showing side chain organization of central lysine residues for D33N and D33S mutants in the presence of inorganic phosphate. Lys-146 hydrogen bonding with Lys-229 requires that one of the lysine residues not be protonated. The hydrogen bond between Lys-146 and Glu-187 preferentially stabilizes the protonated form of Lys-146. Lys-107 is significantly disordered and interacts primarily with the Asp-109 backbone carbonyl (shown in Figure 4). In the D33N−P_i structure, the occupancy of the Lys-146 side chain was set to 0.66 and the remaining electron density was filled with partially occupied water molecules (red spheres) (A). In the D33S−P_i structure, the Lys-146 side chain was refined as a single conformer interacting with Lys-229 (B). Difference electron densities (A and B) were calculated from 2.05 Å (D33N−P_i) and 1.94 Å (D33S−P_i) resolution simulated annealing $F_o - F_c$ omit maps encompassing Lys-229, Lys-146, Lys-107, and alternate water molecules and contoured at 2.8σ.

the Asp-33 mutants is due to a perturbed C-terminal active site attachment that compromises proton transfer at the level of the covalent intermediates. In the presence of phosphate ions, C-terminal active site attachment is stabilized in the crystalline state for subunit D of the native enzyme where C-terminal mobility is not conformationally restricted by crystal packing contacts (*13*). When crystal packing hinders C-terminal movement, as in subunits A and C, phosphate does not induce C-terminal attachment and phosphate attaches at a second anion binding site, located ~2 Å from the first site near the active site periphery

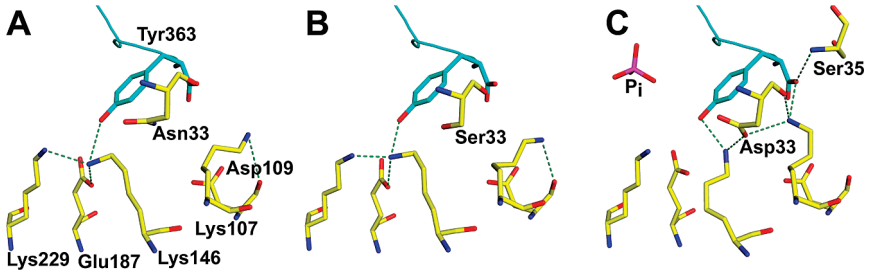

FIGURE 4: C-Terminal docking in the rabbit muscle aldolase active site in the presence of inorganic phosphate and modeled onto the active sites of D33N and D33S mutants. Active site interaction by the rabbit muscle aldolase C-terminus in D33N−P_i (A) and D33S−P_i (B) structures was modeled by superposition based on C-terminal active site interaction (colored cyan) observed in the WT−P_i structure (C). In each case, the Tyr-363 hydroxyl can interact with protonated Lys-146 while interaction of Lys-107 with the Tyr-363 carboxylate in the mutant structures would be accomplished by side chain rotation of Lys-107 thereby breaking the interaction of Lys-107 with the Asp-109 backbone carbonyl. Interaction between the Tyr-363 carboxylate and Ser-35, present in the native enzyme, is however precluded in the mutant structures. The phosphate (P_i) position shown bound in the native enzyme (C) is not occupied in the mutant enzymes.

(*13*). In subunit B, both phosphate binding sites were partially occupied due to equilibration of the C-terminal region between the active site locus and crystal lattice contacts remote from the active site.

Comparison of the refined mutant structures with the native enzyme structure showed no significant conformational differences in any subunit. In both mutants, C-terminus binding in the active site was not observed, with the C-terminal region remaining distant from the active site as observed in the free native enzyme; phosphate binding was observed only at the second anion binding site near the active site periphery. Spatial disposition of the helical regions of residues 34−65 and 302−315 in the presence of phosphate was indistinguishable with respect to the same regions in the free mutant structure. In the native enzyme, these helical regions undergo conformational displacement upon phosphate binding, enabling residues of the helical region of residues 34−65 to contact the C-terminal residues and assist in stabilizing the active site interaction by the C-terminus (*13*).

Lys-146 adopts a novel conformation in the mutant structures soaked with phosphate by interacting with Lys-229 (Figure 3A, B), while Lys-107 displays increased mobility compared to that of the native enzyme (Table 4). In the D33N−P_i structure, occupancy of Lys-146 interacting with Lys-229 was set to 0.66. Inspection of electron density difference maps showed rounded elongated density features, proximal to Lys-146, suggestive of alternate conformations for Lys-146 or the presence of partially occupied water molecules. Electron density features interpreted in terms of partially occupied water molecules are shown for the Asn-33 mutant in Figure 3A. Interaction of Lys-146 with Lys-229 is consistent with hydrogen bond formation (2.75 ± 0.16 and 2.46 ± 0.16 Å for D33N and D33S, respectively) and implies that one of the residues must be unprotonated. Lys-146 in this interaction forms an additional hydrogen bond with Glu-187 (2.75 ± 0.08 Å in both mutant structures) that would stabilize preferentially the positive charge on Lys-146 (Figure 3A,B).[2]

To gain insight into the absence of C-terminal binding with the active site, the C-terminal region bound in the active site from the WT−P_i structure was superimposed onto each mutant structure and compared. Modeling of the C-terminal region into each mutant active site did not create steric hindrance, and interactions made with side chains of active site residues, including those of the flanking helical region (residues 34−52), were conserved or required only minor adjustments to reestablish interactions observed in the WT−P_i structure; exceptions were the C-terminal interactions with Ser-35 and Lys-107. In the native enzyme, Lys-107 interacts with the carboxylate of Tyr-363 (Figure 4C), while in the mutant structures, it is not oriented to make such an interaction due to its hydrogen bonding with the backbone carbonyl of Asp-109 (Figure 4A,B). Although interaction of Lys-107 with Tyr-363 would be possible in the mutant structures, the interaction would require breaking of the Lys-107−Asp-109 interaction and reorientation of the Lys-107 side chain. Moreover, the Tyr-363 carboxylate forms an additional hydrogen bond with the backbone amide of Ser-35 in the WT−P_i enzyme (Figure 4C) which cannot be satisfied in either mutant structure. The helix bearing Ser-35 does not undergo sufficient conformational displacement, precluding interaction between Ser-35 and Tyr-363 in the mutant structures. The ability to anchor the conformational displacement of the flanking helical region for C-terminal interaction is a direct consequence of the negative charge on Asp-33, which is located at the N-terminus of the flanking helix, to form an electrostatic interaction with both Lys-107 and Lys-146 in the WT−P_i structure and a strong charged hydrogen bond with the C3 hydroxyl in the enamine and Schiff base complex. In the mutants, the same interaction is either weaker, in the case of Asn-33, or nonexistent, for Ser-33.

C-Terminal Energetics. The contribution of Asp-33 to proton exchange in Schiff base−enamine interconversion may be estimated from the carbanion oxidation data of the D33N mutant. In this mutant, where proton transfer is nearly rate limiting, mechanistic description of carbanion oxidation simplifies to two elementary rate steps: the rate of C-terminal active site docking and subsequent proton transfer by Tyr-363 that is facilitated by Lys-146. The D33N mutation perturbs both rate steps by affecting C-terminal docking through reduced affinity of Tyr-363 for the active site and by compromising stereospecific proton transfer as Lys-146 in neutral form would be unable to electrostatically stabilize the transient phenolate ion of Tyr-363. The ~300-fold reduction in the overall rate of proton transfer in the D33N mutant translates into an overall heightened kinetic barrier to C-terminal docking and proton transfer of ~3.3 kcal/mol. From a structural perspective, occupancies of less than

[2]In both unliganded D33N and D33S mutant structures, Lys-146 participates in similar hydrogen bonding with Lys-229 and Glu-187 and exhibits several side chain conformers. Schiff base formation would be inhibited by virtue of the hydrogen bond formed between Lys-146 and Lys-229 sequestering the Lys-229 Nζ lone pair and making it unavailable for nucleophilic attack. The combined population of alternate conformers would nevertheless permit a significant fraction (~50%) of Lys-229 to participate in Schiff base formation.

0.2 by the C-terminal region in the active site are generally difficult to discern from electron density maps and correspond to a heightened barrier of > 1.0 kcal/mol in C-terminal affinity for the active site as compared to the native enzyme where the C-terminal region fully occupies the active site in the presence of phosphate in subunit D. From these estimates, the proton transfer rate catalyzed by Tyr-363 is < 50-fold with respect to the native enzyme, consistent with a reduction in pK_a where Lys-146 has nevertheless some residual electrostatic character to promote proton transfer. Such a change in pK_a would indicate an analogous reduction in the rate of proton transfer during C3−C4 bond cleavage as it is also depends on charge stabilization by Lys-146.

From the structural data, charge destabilization in the D33S mutant, contrary to the D33N mutant, does not demand both lysine residues be unprotonated for Tyr-363 interaction. A greater population of lysine residues competent for Tyr-363 interaction in the D33S mutant would argue in favor of more efficient C-terminal interaction and proton transfer. This interpretation is not inconsistent with a slightly greater carbanion oxidation rate and corresponding smaller KIE for the D33S mutant (Table 2) that indicates proton transfer is only partially rate limiting compared to the D33N mutant.

Multiple Catalytic Roles for Asp-33. The biochemical and structural data point to several essential functions for Asp-33 that each facilitate catalysis. Its negative charge serves to stabilize the protonated forms of the proximal lysine residues, Lys-107 and Lys-146, and to spatially orient their side chains, resulting in competent active site binding and efficient proton transfer by C-terminal Tyr-363. When the level of side chain disorder of the lysine residues is reduced, the entropic penality incurred to align these residues for C-terminal interaction is minimized. This interpretation is consistent with protein−protein binding surfaces having greater rigidity so that the entropic cost is minimized on binding, whereas surrounding residues can form a more flexible cushion (*50*). Asp-33 also anchors a requisite conformational change by the flanking helix (residues 34−65) through its strong charged interaction with the DHAP C3-OH group, enabling the Tyr-363 carboxylate to hydrogen bond with Ser-35, which contributes to C-terminal active site binding. Furthermore, Asp-33 in promoting the protonated form of Lys-146 ensures stabilization of the developing negative charges at the C4 hydroxyl during C3−C4 bond cleavage and at the Tyr-363 phenolate during stereospecific proton transfer. Estimates indicate that the reductions associated with the rates of proton transfer and C-terminal docking in the active site are comparable, albeit moderate in extent (< 50-fold). The cumulative effect of these reductions is, however, significant with respect to enzymatic activity and highlights the critical role of Asp-33 in aldolase catalysis. These factors explain the low observed rate of substrate turnover in the Asp-33 mutants and that it is smaller with respect to carbanion oxidation.

ACKNOWLEDGMENT

Assistance by NSLS X8C and X12B beamline personnel, Drs. L. Flaks, D. K. Schneider, and A. Soares, was appreciated. Critical reading of the manuscript by Dr. Stephen Seah is gratefully acknowledged. Technical assistance in structure refinement and preparation of manuscript figures was generously provided by Guillaume Arthus-Cartier.

REFERENCES

1. Grazi, E., Rowley, P. T., Chang, T., Tchola, O., and Horecker, B. L. (1962) The mechanism of action of aldolases. III. Schiff base formation with lysine. *Biochem. Biophys. Res. Commun. 9*, 38–43.
2. Rose, I. A., and Rieder, S. V. (1958) Studies on the mechanism on the aldolase reaction: Isotope exchange reactions of muscle and yeast aldolase. *J. Biol. Chem. 231*, 315–329.
3. Penhoet, E. E., and Rutter, W. J. (1971) Catalytic and immunochemical properties of homomeric and heteromeric combinations of aldolase subunits. *J. Biol. Chem. 246*, 318–323.
4. Gefflaut, T., Blonski, C., Perie, J., and Willson, M. (1995) Class I aldolases: Substrate specificity, mechanism, inhibitors and structural aspects. *Prog. Biophys. Mol. Biol. 63*, 301–340.
5. Rose, I. A., and Warms, J. V. B. (1985) Complexes of muscle aldolase in equilibrium with fructose 1,6-bisphosphate. *Biochemistry 24*, 3952–3957.
6. Ray, B. D., Harper, E. T., and Fife, W. K. (1983) Carbon-13 NMR evidence of carbinolamine formation at the active site of an imine-forming aldolase. *J. Am. Chem. Soc. 105*, 3731–3732.
7. Jencks, W. P. (1969) *Catalysis in Chemistry and Enzymology*, pp 120−121, McGraw-Hill Book Co., New York..
8. Grazi, E., Cheng, T., and Horecker, B. L. (1962) The formation of a stable aldolase-dihydroxyacetone phosphate complex. *Biochem. Biophys. Res. Commun. 7*, 250–253.
9. Rose, I. A. (1958) The Absolute Configuration of Dihydroxyacetone Phosphate Tritiated by Aldolase Reaction. *J. Am. Chem. Soc. 80*, 5835–5836.
10. Hannaert, V., Bringaud, F., Opperdoes, F. R., and Michels, P. A. (2003) Evolution of energy metabolism and its compartmentation in Kinetoplastida. *Kinetoplastid Biol. Dis. 2*, 11–41.
11. Sygusch, J., Beaudry, D., and Allaire, M. (1987) Molecular architecture of rabbit skeletal muscle aldolase at 2.7-Å resolution. *Proc. Natl. Acad. Sci. U.S.A. 84*, 7846–7850.
12. St-Jean, M., Lafrance-Vanasse, J., Liotard, B., and Sygusch, J. (2005) High resolution reaction intermediates of rabbit muscle fructose-1,6-bisphosphate aldolase: Substrate cleavage and induced fit. *J. Biol. Chem. 280*, 27262–27270.
13. St-Jean, M., and Sygusch, J. (2007) Stereospecific proton transfer by a mobile catalyst in mammalian fructose-1,6-bisphosphate aldolase. *J. Biol. Chem. 282*, 31028–31037.
14. Blom, N., and Sygusch, J. (1997) Product binding and role of the C-terminal region in class I D-fructose 1,6-bisphosphate aldolase. *Nat. Struct. Biol. 4*, 36–39.
15. Hester, G., Brenner-Holzach, O., Rossi, F. A., Struck-Donatz, M., Winterhalter, K. H., Smit, J. D., and Piontek, K. (1991) The crystal structure of fructose-1,6-bisphosphate aldolase from *Drosophila melanogaster*, at 2.5 Å resolution. *FEBS Lett. 292*, 237–242.
16. Lafrance-Vanasse, J., and Sygusch, J. (2007) Carboxy-Terminus Recruitment Induced by Substrate Binding in Eukaryotic Fructose Bis-phosphate Aldolases. *Biochemistry 46*, 9533–9540.
17. Drechsler, E. R., Boyer, P. D., and Kowalsky, A. G. (1959) The catalytic activity of carboxypeptidase-degraded aldolase. *J. Biol. Chem. 234*, 2627–2634.
18. Rose, I. A., O'Connell, E. L., and Mehler, A. H. (1965) Mechanism of the aldolase reaction. *J. Biol. Chem. 240*, 1758–1765.
19. Dax, C., Coincon, M., Sygusch, J., and Blonski, C. (2005) Hydroxynaphthaldehyde phosphate derivatives as potent covalent Schiff base inhibitors of fructose-1,6-bisphosphate aldolase. *Biochemistry 44*, 5430–5443.
20. Morris, A. J., and Tolan, D. R. (1993) Site-directed mutagenesis identifies aspartate 33 as a previously unidentified critical residue in the catalytic mechanism of rabbit aldolase A. *J. Biol. Chem. 268*, 1095–1100.
21. Berthiaume, L., Tolan, D. R., and Sygusch, J. (1993) Differential usage of the carboxyl-terminal region among aldolase isozymes. *J. Biol. Chem. 268*, 10826–10835.
22. Morris, A. J., and Tolan, D. R. (1994) Lysine-146 of rabbit muscle aldolase is essential for cleavage and condensation of the C3−C4 bond of fructose 1,6-bis(phosphate). *Biochemistry 33*, 12291–12297.
23. Maurady, A., Zdanov, A., de Moissac, D., Beaudry, D., and Sygusch, J. (2002) A Conserved Glutamate Residue Exhibits Multifunctional Catalytic Roles in D-Fructose-1,6-bisphosphate Aldolases. *J. Biol. Chem. 277*, 9474–9483.
24. Baranowski, T., and Niederland, T. R. (1949) Aldolase activity of myogen A. *J. Biol. Chem. 180*, 543–551.
25. Racker, E. (1947) Spectrophotometric measurement of hexokinase and phosphohexokinase activity. *J. Biol. Chem. 167*, 843–854.
26. Spolter, P. D., Adelman, R. C., and Weinhouse, S. (1965) Distinctive properties of native and carboxypeptidase-treated aldolases of rabbit muscle and liver. *J. Biol. Chem. 244*, 126–134.

27. Leatherbarrow, R. J. (1992) *GraFit*, version 3.0, Erithacus Software Ltd., Horley, U.K..
28. Healy, M. J., and Christen, P. (1973) Mechanistic probes for enzymatic reactions. Oxidation-reduction indicators as oxidants of intermediary carbanions (studies with aldolase, aspartate aminotransferase, pyruvate decarboxylase, and 6-phosphogluconate dehydrogenase). *Biochemistry 12*, 35–41.
29. Berthiaume, L., Loisel, T. P., and Sygusch, J. (1991) Carboxyl terminus region modulates catalytic activity of recombinant maize aldolase. *J. Biol. Chem. 266*, 17099–17105.
30. Page, P., Blonski, C., and Périé, J. (1998) Interaction of phosphonomethyl analog of dihydroxyacetone phosphate with rabbit muscle aldolase. *Biochim. Biophys. Acta 1386*, 59–64.
31. Page, P., Blonski, C., and Périé, J. (1999) Origin of the slow-binding inhibition of aldolase by D-glycer-tetrulose 1-phosphate (D-Erythrulose 1-phosphate) from the comparison with the isosteric phosphonate analog. *Eur. J. Org. Chem. 1999*, 2853–2857.
32. Otwinowski, Z., and Minor, W. (1997) Processing of X-ray diffraction data collected in oscillation mode. *Methods Enzymol. 276*, 307–326.
33. Brunger, A. T., Adams, P. D., Clore, G. M., DeLano, W. L., Gros, P., Grosse-Kunstleve, R. W., Jiang, J.-S., Kuszewski, J., Nilges, N., Pannu, N. S., Read, R. J., Rice, L. M., Simonson, T., and Warren, G. L. (1998) Crystallography & NMR system: A new software suite for macromolecular structure determination. *Acta Crystallogr. D54*, 905–921.
34. Jones, T. A., Zou, J. Y., Cowan, S. W., and Kjeldgaard, M. (1991) Improved methods for building protein models in electron density maps and the location of errors in these models. *Acta Crystallogr. A47*, 110–119.
35. Schuttelkopf, A. W., and van Aalten, D. M. (2004) PRODRG: A tool for high-throughput crystallography of protein-ligand complexes. *Acta Crystallogr. D60*, 1355–1363.
36. Laskowski, R. A., MacArthur, M. W., Moss, D. S., and Thornton, J. M. (1993) PROCHECK: A program to check the stereochemical quality of protein structures. *J. Appl. Crystallogr. 26*, 283–290.
37. DeLano, W. L. (2002) *The PyMOL Molecular Graphics System*, DeLano Scientific, San Carlos, CA..
38. Emsley, P., and Cowtan, K. (2004) Coot: Model-building tools for molecular graphics. *Acta Crystallogr. D60*, 2126–2132.
39. Vijayakumar, M., Qian, H., and Zhou, H. X. (1999) Hydrogen bonds between short polar side chains and peptide backbone: Prevalence in proteins and effects on helix-forming propensities. *Proteins 34*, 497–507.
40. Grazi, E. (1975) Fructose 1,6-diphosphate aldolase from rabbit muscle. Effect of pH on the rate of formation and on the equilibrium concentration of the carbanion intermediate. *Biochem. J. 151*, 167–172.
41. Azema, L., Lakhdar-Ghazal, F., Sygusch, J., and Blonski, C. (2003) Characterization of proton abstraction steps in enzymatic reactions by Fourier transform infrared spectroscopy. *Anal. Biochem. 318*, 142–145.
42. Biellmann, J. F., O'Connell, E. L., and Rose, I. A. (1969) Secondary isotope effects in reactions catalyzed by yeast and muscle aldolase. *J. Am. Chem. Soc. 91*, 6484–6488.
43. Creighton, T. E. (1993) *Proteins: Structure and Molecular Properties*, 2nd ed., Freeman, New York..
44. Williamson, M. P., and Williams, D. H. (1984) Hydrophobic interactions affect hydrogen bond strengths in complexes between peptides and vancomycin or ristocetin. *Eur. J. Biochem. 138*, 345–348.
45. Harris, T. K., and Turner, G. J. (2002) Structural basis of perturbed pK_a values of catalytic groups in enzyme active sites. *IUBMB Life 53*, 85–98.
46. Hartman, F. C., and Brown, J. P. (1976) Affinity labeling of a previously undetected essential lysyl residue in class I fructose bisphosphate aldolase. *J. Biol. Chem. 251*, 3057–3062.
47. Warren, S., Zerner, B., and Westheimer, F. H. (1966) Acetoacetate decarboxylase. Identification of lysine at the active site. *Biochemistry 5*, 817–823.
48. Schmidt, D. E., and Westheimer, F. H. (1971) pK of the lysine amino group at the active site of acetoacetate decarboxylase. *Biochemistry 10*, 1249–1253.
49. Highbarger, L. A., Gerlt, J. A., and Kenyon, G. L. (1996) Mechanism of the reaction catalyzed by acetoacetate decarboxylase. Importance of lysine 116 in determining the pKa of active-site lysine 115. *Biochemistry 35*, 41–46.
50. Ma, B., Elkayam, T., Wolfson, H., and Nussinov, R. (2003) Protein−protein interactions: Structurally conserved residues distinguish between binding sites and exposed protein surfaces. *Proc. Natl. Acad. Sci. U.S.A. 100*, 5772–5777.